Available online at www.sciencedirect.com

ScienceDirect

journal homepage: www.elsevier.com/locate/he

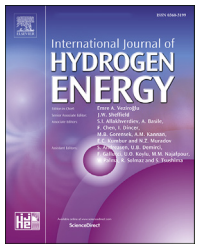

Modelling of methane sorption enhanced reforming for blue hydrogen production in an adiabatic fixed bed reactor: unravelling the role of the reactor's thermal behavior

Abdelrahman Mostafa [a], *Irene Rapone* [b], *Aldo Bosetti* [b], *Matteo C. Romano* [c], *Alessandra Beretta* [a], *Gianpiero Groppi* [a,*]

[a] *LCCP – Laboratory of Catalysis and Catalytic Processes, Dipartimento di Energia, Politecnico di Milano, Via La Masa 34, 20156, Milano, Italy*

[b] *Renewable, New Energies and Material Science Research Center, Eni SpA, Via Fauser 4, 28100, Novara, Italy*

[c] *GECOS – Group of Energy Conversion Systems, Dipartimento di Energia, Politecnico di Milano, Via Lambruschini 4, 20156, Milano, Italy*

HIGHLIGHTS

- Dynamic heterogeneous model reveals the thermal behavior of the SER process.
- Strategies to cover the energy demand for efficient H_2 production are assessed.
- SER allows single step production of >95% purity hydrogen with >85% carbon capture rate.
- Potential to avoid the cooling step between regeneration and reforming stages is demonstrated.

ARTICLE INFO

Article history:
Received 18 July 2022
Received in revised form
7 February 2023
Accepted 23 March 2023
Available online 17 April 2023

Keywords:
Modelling
CO_2 capture
Hydrogen production
Sorption enhanced reforming
Adiabatic reactor

ABSTRACT

Methane sorption enhanced reforming (SER) is investigated in this work as a promising route for blue H_2 production. A 1-D dynamic heterogeneous model is developed to evaluate the thermal behavior of a fixed bed reactor under adiabatic conditions. The heterogeneous model allows to decouple the feed gas temperature from the initial solid one in order to investigate the behavior of the reforming step in a temperature swing reforming/regeneration process. The effects of the feed gas temperature, the initial bed temperature, and the bed thermal capacity are studied by evaluating the global impact of each parameter through a set of key performance indices (CH_4 conversion, H_2 yield and purity, carbon capture ratio) calculated as integrals over the duration of the reforming step. The results highlight the minor effect of the initial bed temperature on the process performances showing the potential of minimizing the extent of a cooling step between regeneration and reforming stages. Besides, due to the endothermic nature of the methane sorption enhanced reforming process at high temperatures, thermal energy must be provided to the SER process to achieve high CH_4 conversion and high carbon capture ratio. This can be made either in the form of high feed temperature or by utilizing the energy stored in the bed benefiting from the bed thermal capacity.

© 2023 The Authors. Published by Elsevier Ltd on behalf of Hydrogen Energy Publications LLC. This is an open access article under the CC BY license (http://creativecommons.org/licenses/by/4.0/).

* *Corresponding author.*
E-mail address: gianpiero.groppi@polimi.it (G. Groppi).

https://doi.org/10.1016/j.ijhydene.2023.03.357

0360-3199/© 2023 The Authors. Published by Elsevier Ltd on behalf of Hydrogen Energy Publications LLC. This is an open access article under the CC BY license (http://creativecommons.org/licenses/by/4.0/).

Introduction

Hydrogen plays an important role both as an energy vector used for energy storage, transportation, and power production, or as a raw material in the chemical and petroleum industries [1]. However, the major part of the hydrogen is currently produced from fossil fuels either methane through the steam reforming (SR), autothermal reforming of natural gas, or through partial oxidation of heavier cuts [2]. By examining the latest IEA energy outlook [3], the role of fossil based natural gas is evident where even in the most optimistic scenario, natural gas will remain a major player in the global energy mix for the projected period until 2050. The rapid development of processes capable of utilizing the fossil-based methane with the flexibility to work with future green feedstocks while limiting the carbon emissions resulting in net zero emissions is of the utmost importance to achieve the net zero targets. Among the several emerging technologies suggested for this application, Sorption Enhanced Reforming (SER) is very promising. Several experimental and modelling studies were performed on the SER of methane commonly using conventional steam reforming Ni based catalysts coupled with CO_2 sorbents [4–9]. CaO based sorbents are especially suitable for methane SER since they provide high sorption capacity and fast kinetics in the high temperature range [10,11] coupled with high availability and cost competitiveness [12]. In the presence of CaO, the CO_2 produced by the consecutive methane steam reforming and water gas shift (WGS) reactions (Eqs. (1) and (2)) is captured through the carbonation reaction, Eq. (3). Being a highly exothermic reaction, the CaO carbonation tends to balance the highly endothermic nature of methane steam reforming.

$$CH_4 + H_2O \leftrightarrow CO + 3H_2 \qquad \Delta H^{\circ}_{298K} = 206\ kJmol^{-1} \tag{1}$$

$$CO + H_2O \leftrightarrow CO_2 + H_2 \qquad \Delta H^{\circ}_{298K} = -41\ kJmol^{-1} \tag{2}$$

$$CaO + CO_2 \leftrightarrow CaCO_3 \qquad \Delta H^{\circ}_{298K} = -178\ kJmol^{-1} \tag{3}$$

The CO_2 sorption reaction, being a gas solid reaction dependent on the availability of active sorbent, makes the process dynamic in the fixed bed arrangement [13]. A typical arrangement of the process can approach a continuous steady production of hydrogen through alternating parallel reactors between the two steps of the process: the sorption enhanced reforming and the sorbent regeneration passing through the two intermediate steps of blow down and repressurization. As previously explained, the reforming reaction, being a highly endothermic reaction with an increasing number of moles, is favored at high temperature and low pressure. On the other side, the sorption reaction is favored at low temperature and high pressure. This interplay between the two reactions and the aim of improving the global efficiency of a hydrogen production plant focuses on maintaining the SER reactor at the lowest feasible temperature and the highest possible pressure, delivering a stream of pure pressurized hydrogen to be easily utilized in the downstream processes while achieving high energy efficiency. Regarding the regeneration step, being a highly endothermic reaction with an increasing number of moles, the CaO calcination reaction is favored at high temperature and low pressure. It was shown in the literature [14] that a definite CO_2 partial pressure, function of temperature, establishes in the gas phase at chemical equilibrium making the regeneration of this sorbent suitable by both pressure and temperature swing desorption.

Several modelling activities are available in the literature for methane sorption enhanced reforming process in a fixed bed reactor. Xiu et al. [15] developed a model of the complete SER process including the reaction/sorption and regeneration steps. Lee et al. [16] presented a 1-D pseudo homogeneous model describing the steps of the transient behavior of the SER process in a lab scale reactor placed inside an oven to keep a fixed reactor wall temperature. Following the same concept, Li and Cai [17] developed a kinetic expression for the cyclic CaO carbonation and calcination reactions and implemented their kinetic expressions in a 1-D pseudo homogeneous fixed bed reactor model keeping the reactor wall temperature constant. More recently, Sheu et al. [18] studied the transient behavior of an externally heated SER reactor using a 2D model. Moving to the large-scale applications, Fernandez et al. [19] presented a 1-D pseudo homogeneous model of a large-scale adiabatic fixed bed reactor. The result of this work proves the theoretical feasibility of applying the SER process for a large-scale hydrogen production plant. Based on the works of Fernandez et al., Abbas et al. [20,21] proposed a 1-D heterogenous model of an adiabatic packed bed reactor for both high pressure, large scale applications similar to the conditions modelled by Fernandez et al. [19] and small scale low pressure applications. Recently, Martini et al. [22,23] integrated the SER process using a 1-D pseudo homogenous fixed bed reactor model within their work in developing a process for large scale production of H_2 coupled with CO_2 capture.

However, pseudo-homogeneous models do not allow decoupling of the temperature level of the gas from that of the solid phases, which can play an important role in the optimization of the reforming/regeneration temperature cycle. Additionally, the heterogeneous model can properly address the progressive conversion of the sorbent from CaO to $CaCO_3$, which increases the mass of the bed and changes its specific heat capacity, thereby affecting the thermal behavior of the reactor and the performances of the process.

In this work we present a 1-D heterogenous model for the methane SER process in an adiabatic fixed bed reactor. The model includes three well mixed solid phases: the sorbent, the catalyst, and the inert, in addition to the gas phase. The separation of the different phases of the reactor (gas, catalyst, sorbent, and inert) highlights the interplay between them and their impact on the thermal behavior of the reactor and the global performance of the SER process. The role of the heat capacity of the reactor is studied in detail including the sorbent variable density and specific heat capacity effect. The model is used to perform simulations with decoupled initial bed and feed gas temperatures, in order to investigate the behavior of the reforming step in a temperature swing cycle. The performances of the SER process are evaluated on the basis of several key performance indices defined in the work. From the obtained results, a strategy to improve the methane conversion and hydrogen yield is proposed, based on

introducing the high-density inert material in the reactor and thus increasing the bed heat capacity. Results of this proposed strategy are compared with the common SER arrangement and show improved methane conversion, hydrogen yield, and carbon capturing ratio in the adiabatic condition.

Methods

In this section, the reactor model is described providing all the correlations used. A scheme of the reactor is given in Fig. S1 of section A of the Supplementary Material.

SER reactor model

A heterogeneous one-dimensional dynamic model of a fixed bed reactor was developed using gPROMS® software platform. The model describes the time evolution of concentration and temperature axial profiles of the sorption/reforming step of a SER cycle. The model includes 1D total mass balance for gas phase, 1D i-species mass balances ($i = CH_4, H_2O, H_2, CO, CO_2, N_2$) and energy balances for the gas-phase, catalyst, and sorbent solid phases. The pressure drop, along the reactor was evaluated by using the Ergun equation for fixed beds (E. (4)) [24].

$$\frac{dP}{dz} = -\left(\frac{150(1-\varepsilon)^2}{d_p^2\varepsilon^3}\mu_g u + \frac{1.75(1-\varepsilon)}{d_P\varepsilon^3}\rho_g u^2\right) \tag{4}$$

The reactor bed void fraction is calculated as defined in Equation S1 of section B of the Supplementary Material.

Mass balance equations:

The total mass balance for the gas phase (E. (5)) consists of four terms: mass accumulation, axial mass convection, mass exchange between gas and catalyst phases, and mass exchange between the gas and the sorbent phases.

$$\frac{\varepsilon}{u}\frac{\partial G}{\partial t} = -\frac{\partial(G)}{\partial z} + a_{V,sorbent}\sum_{i}^{NC} MW_i k_{m,i}\left(C_{sorbent,i} - C_{gas,i}\right) + a_{V,catalyst}\sum_{i}^{NC} MW_i k_{m,i}\left(C_{catalyst,i} - C_{gas,i}\right) \tag{5}$$

Solid surface area per unit volume (Eqs. (6) and (7)) depends on the solid phase considered (catalyst or sorbent) and it was weighted with the volumetric fraction ξ related to the specific solid phase ($\xi_{catalyst} + \xi_{sorbent} = 1$). This scheme was applied to all the balance equations.

$$a_{V,catalyst} = (1-\varepsilon)\xi_{catalyst}\frac{S_{P,catalyst}}{V_P, catalyst} \tag{6}$$

$$a_{V,sorbent} = (1-\varepsilon)\xi_{sorbent}\frac{S_{P,sorbent}}{V_P, sorbent} \tag{7}$$

Gas phase molar balances for i-species (Eq. (8)) consist of five terms: molar accumulation, axial convection, axial molar dispersion, mass transfer between the gas and the catalyst phases, and between the gas and the sorbent phases.

$$\varepsilon\frac{\partial C_{gas,i}}{\partial t} = -\frac{\partial\left(uC_{gas,i}\right)}{\partial z} + D_{ae,i}\frac{\partial^2\left(C_{gas,i}\right)}{\partial z^2} + a_{V,catalyst}k_{m,i}\left(C_{catalyst,i} - C_{gas,i}\right) + a_{V,sorbent}k_{m,i}\left(C_{sorbent,i} - C_{gas,i}\right) \tag{8}$$

Regarding the catalyst phase no accumulation on the surface was considered and continuity equations for the i-species at the gas-catalyst interface (Eq. (9)) consist of two terms: mass transfer between the gas and catalyst phase, and rate of species consumption or production. Similarly, the continuity equation for the CO_2 species at the gas-sorbent interface (Eq. (10)) equals the mass transfer rate between the gas and sorbent phase and the rate of CO_2 consumption by sorption, which is governed by the rate of the sorbent conversion. Assuming ideal selectivity of the sorbent for CO_2, no molar fluxes between the gas phase and the sorbent phase were considered for all the i-species except CO_2. Finally, a sorbent balance equation (Eq. (11)) consistent with the continuity one was considered.

A global catalyst effectiveness factor (η) was included in the i-species mass balance similarly to works presented in the literature [15–17,19,20,25] to account for the intra particle diffusion limitations in the catalyst particle. A constant value of the effectiveness factor equal to 0.3 was selected based on the modelling and experimental work presented in [16] using similar small particle size.

$$a_{V,catalyst}k_{m,i}\left(C_{gas,i} - C_{catalyst,i}\right) = \eta(1-\varepsilon)\xi_{catalyst}\rho_{catalyst}\sum\nolimits_j \nu_{ij}R_j \tag{9}$$

$$a_{V,sorbent}k_{m,i}\left(C_{gas,i} - C_{sorbent,i}\right) = (1-\varepsilon)\xi_{sorbent}\rho_{CaO}\,\nu_{icarb}R_{carb} \tag{10}$$

$$\frac{dX_{sorbent}}{dt} = MW_{CaO}R_{carb} \tag{11}$$

Energy balance equations:

The energy balance of the gas phase (Eq. (12)) consists of six terms: gas heat accumulation; axial thermal convection; axial heat dispersion; heat transfer between the gas and the catalyst phases; heat exchange between the gas and sorbent phases.

$$\varepsilon\rho_g cp_g\frac{\partial T_{gas}}{\partial t} = -u\rho_g cp_g\frac{\partial T}{\partial z} + \lambda_{ax}\frac{\partial^2 T}{\partial z^2} + a_{V,catalyst}h_{gs}\left(T_{catalyst} - T_{gas}\right) + a_{V,sorbent}h_{gs}\left(T_{sorbent} - T_{gas}\right) \tag{12}$$

The catalyst phase energy balance (Eq. (13)) and the sorbent phase energy balance (Eq. (14)) consist of three terms each: catalyst/sorbent heat accumulation; heat exchange between the gas and catalyst/sorbent phase; enthalpy release by the reactions (catalytic or CO_2 sorption).

$$(1-\varepsilon)\xi_{catalyst}\rho_{catalyst}cp_{catalyst}\frac{\partial T_{catalyst}}{\partial t} = a_{V,catalyst}h_{gs}\left(T_{gas} - T_{catalyst}\right) - (1-\varepsilon)\xi_{catalyst}\rho_{catalyst}\sum\eta R_j\Delta H_{R,j} \tag{13}$$

$$(1-\varepsilon)\xi_{sorbent}\rho_{sorbent}cp_{sorbent}\frac{\partial T_{sorbent}}{\partial t} = a_{V,sorbent}h_{gs}\left(T_{gas} - T_{sorbent}\right) - (1-\varepsilon)\xi_{sorbent}\rho_{CaO}R_{carb}\Delta H_{carb} \tag{14}$$

The particle density of the catalyst was taken as constant while the particle density of the sorbent was considered variable in time and space, depending on the sorbent conversion as presented in Eq. (15). This analogy is based on the model proposed by Bhatia and Perlmutter [26] where the solid product $CaCO_3$ occupies larger volume than the consumed CaO leading to a progressive decrease of the porosity and an increase of the solid particle density at constant particle diameter.

Additionally, the overall heat capacity of the sorbent was calculated as an average of both species, CaO and $CaCO_3$, following (Eq. (16)).

$$\rho_{sorbent} = \rho_{CaO}{}^{*}\left(1 - X_{sorbent} + X_{sorbent}{}^{*}\frac{MW_{CaCO_3}}{MW_{CaO}}\right) \tag{15}$$

$$Cp_{sorbent} = Cp_{CaO}(1 - X_{sorbent}) + Cp_{CaCO_3}X_{sorbent} \tag{16}$$

To evaluate the role of the heat capacity of the bed, the case was also simulated of highly dense inert particles introduced into the solid bed to increase the overall bed heat capacity, although occupying a small volume fraction. At this scope, since no reactions take place on the inert surface, only one additional equation describing the inert phase energy balance was added to the model (Eq. (18)). Besides, the gas phase energy balance was modified to include the heat transfer between the gas and the inert phases (Eq. (19)). Additionally, the volumetric fraction ξ_{inert} was added so that $(\xi_{catalyst} + \xi_{inert} + \xi_{sorbent} = 1)$.

$$a_{V,inert} = (1 - \varepsilon)\xi_{inert}\frac{S_{P,inert}}{V_P,\, inert} \tag{17}$$

$$(1 - \varepsilon)\xi_{inert}\rho_{inert}cp_{inert}\frac{\partial T_{inert}}{\partial t} = a_{V,inert}h_{gs}\left(T_{gas} - T_{inert}\right) \tag{18}$$

$$\begin{aligned}\left(\varepsilon\rho_g Cp_g\right)\frac{\partial T_{gas}}{\partial t} = &- u\rho_g Cp_g\frac{\partial T}{\partial z} + \lambda_{ax}\frac{\partial^2 T}{\partial z^2} + a_{V,catalyst}h_{gs}\left(T_{catalyst} - T_{gas}\right)\\ &+ a_{V,sorbent}h_{gs}\left(T_{sorbent} - T_{gas}\right) + a_{V,inert}h_{gs}\left(T_{inert} - T_{gas}\right)\end{aligned} \tag{19}$$

Boundary and initial conditions:

The Danckwerts boundary conditions (Eq. (20)) were imposed at the reactor inlet and outlet.

$$\begin{cases} F_{gas,tot} = C^0_{gas,tot}v^0_{gas} & z = 0\\ C^0_{gas,i} = C_{gas,i} - \dfrac{D_{ae,i}}{v_{gas}}\dfrac{\partial C_{gas,i}}{\partial z} & z = 0\\ T^0_{gas} = T_{gas} - \dfrac{\lambda_{ax}}{v_{gas}Cp_{gas}}\dfrac{\partial T_{gas}}{\partial z} & z = 0\\ \dfrac{\partial C_{gas,i}}{\partial z} = 0 & z = L_t\\ \dfrac{\partial T_{gas}}{\partial z} = 0 & z = L_t \end{cases} \tag{20}$$

The reactor was assumed initially to be filled with a mixture of steam and hydrogen in thermal equilibrium with the solid bed. For all the simulations performed in this work, the initial composition of the gas phase inside the reactor had negligible effect on the results given that all the trapped gas was always completely purged in less than 30 s.

The initial conditions at t = 0 selected for the reactor are presented in Eq. (21).

$$\begin{cases} T_{gas} = T_{solids\ initial} & z < L_t\\ T_{catalyst} = T_{sorbent} = T_{solids\ initial} & 0 \le z \le L_t\\ X_{sorbent} = 0 & 0 \le z \le L_t\\ C_{gas,i} = C^{t=0}_{gas,i} & 0 < z < L_t \end{cases} \tag{21}$$

Physical properties, transport correlations, and reaction kinetics

The physical and chemical properties (molecular weight, specific heat, density, viscosity and thermal conductivity) of the reacting mixture were calculated using the gPROMS® Multiflash 4.3 utility tool, while diffusivities, mass and heat transport coefficients were calculated with correlations taken from the literature [27–31] and reported in Section B of the Supplementary Material.

Concerning thermochemical data, the reactions' enthalpies were calculated with specific heat capacities and enthalpies of formation of all the species from [32]. The effect of the temperature on the reactions' enthalpies was accounted for; indeed, the overall enthalpy of the SER process changes by over 20 kJ/mol from a slightly exothermic −13.5 kJ/mol at the standard temperature (25 °C) to a slightly endothermic +13.2 kJ/mol at the actual temperature of the process (550 °C). More details on enthalpy changes with temperature are reported in Section C of the Supplementary Material.

The C1 kinetic model (including methane reforming, methanation, and water gas shift reactions) used in this work is the one developed by Xu and Froment [33] for nickel catalyst. The rate equations and the kinetic and equilibrium parameters are reported in the Supplementary Material (Section D).

Regarding the description of CaO carbonation, the kinetics were expressed in terms of rate of conversion of the CaO, as commonly found in the literature [34–36]. Many kinetic models were proposed, with different degrees of complexity to capture the specific nature of this reaction. CaO carbonation reaction is known to undergo two consecutive steps: an initially fast kinetically controlled step, followed by a much slower diffusion-controlled step through the growing carbonate layer [35,37,38]. However, as studied by Mess et al. [39] the diffusion mechanism controlling the second step leads to very slow conversion rate that has negligible importance for a practical CO_2 capturing application. For this reason and in line with the scope of this work, the empirical equation presented in [40] and used in the modelling works of Fernandez et al. [19] and Abbas et al. [20,21] was selected for calculating the rate of CO_2 sorption as shown in Eq. (22).

$$R_{carb} = \frac{1}{MW_{CaO}}\frac{\nu_{CO_2\ carb}}{\nu_{CaO\ carb}}k_{carb}\left(y_{co_2} - y_{co_2,eq}\right)\left(X_{max} - X_{sorbent}\right) \tag{22}$$

In Eq. (22) X_{max} represents the maximum sorbent conversion, defined as the value of the conversion at which the carbonation reaction enters in the product layer diffusion regime; many works in the literature showed that X_{max} may decline with the number of cycles depending on the structure of the sorbent and the presence of inert atoms (structural promoters), the regeneration temperature, and the regeneration media [1,10]. However, synthetic calcium based sorbents were developed by several authors to improve the durability [1,41]. Carbonation reactivity also depends on the type of the sorbent used. Synthetic sorbents provide a wide range of reactivities, both higher and lower than the natural one, as reported in [19]. In this work, the use of a synthetic sorbent was assumed, a suitable option

for a commercial application where high number of cycles is expected. Accordingly, the maximum sorbent conversion, X_{max}, was herein considered to be constant and, following the work of Fernandez et al. [19], it was assumed equal to 0.4; the kinetic constant for the carbonation reaction, k_{carb}, was set at 0.35 s^{-1} as a reference value. The equilibrium partial pressure of CO_2 was calculated from Eq. (23) [42].

$$\log\left(p_{co_2,eq}\right) = 7.079 - \frac{38000}{4.574T} \quad (23)$$

Numerical solution scheme

The mathematical SER reactor model was implemented in gPROMS® software platform for the dynamic simulation. The SARDAU solver for differential–algebraic equations systems based on implicit Backward Differentiation Formula (BDF) with variable time step was used for time integration. The integration time step of BDF changes in accordance with a maximum local error criterion implemented in gPROMS®. A first order Backward Finite Difference Method (BFDM) was used for the discretization of the axial reactor coordinate using 140 discretization points along the axial coordinate in an equi-spaced grid. Further increasing of the number of discretization points was checked to have negligible effect on the results. The reporting time interval is set as the default value of 10 s. The consistency of the model results was checked by a evaluating the global carbon material balance and the global enthalpy balance including gas and solid phases. The balance equations can be found in section E of the Supplementary Material. Satisfactory closure of the balances was obtained with a minor error (<1%) within the range of acceptable numerical accuracy.

Results and discussion

In this section, the model is validated against lab-scale data from the literature, then a reference case is discussed defining the key performance indices (KPI) used for evaluating the process. Finally, a parametric analysis is presented showing the effect of the different working conditions on the performance of the SER reactor.

SER model validation against lab-scale data

Following the same procedure as presented by Fernandez et al. [19], the model was first tested by comparison with the experimental results of Balasubramanian et al. [43], performed in packed tube (1.9 cm diameter, 3.8 cm length) externally heated to keep constant the wall temperature at 650 °C. The thermal behavior of the reactor was not discussed by the authors, but it is reasonable to assume that thermal effects were practically negligible in such a small-scale test unit. To properly reproduce this condition, the energy balance of the SER model was modified to account for radial heat transfer (Eqs. S13 and S14 in Section F of Supplementary Material); the overall heat transfer term was sufficiently high to keep the bed almost isothermal during all the phases of the process. Besides, since gas inlet temperature and solid initial temperature were equal in the experimental run, a heterogeneous description was not needed and a single pseudo-homogeneous phase was assumed, by lumping the heat capacity of the gas and the solid phases, which implies that all the phases are at the same temperature for each axial position at any defined time.

Experimental data (symbols) and model predictions (in solid lines) are reported in Fig. 1, in terms of outlet molar fraction on a dry basis of carbon containing species (CH_4, CO, CO_2) and hydrogen. The full set of input data of the simulations (including geometrical and operating parameters) are detailed in Table S2 of Section F of the Supplementary Material.

It is worth observing that the data reported in Fig. 1 were actually preceded by another dynamic evolution, since, as reported by Balasubramanian et al. [43], the experiment included an initial phase (the start-up), during which the feeding mixture filled the reactor and progressively activated the catalyst by reduction; the start of the SER dynamics was thus identified by the authors as the time when an approximately constant CH_4 conversion was reached, and matched with the expected value at SER equilibrium (the pre-breakthrough phase). With time, the breakthrough of progressively increasing amount of CO_2 in the outlet stream was observed (breakthrough phase), which was associated with the approach to the saturation of sorbent with loss of CO_2 capture efficiency; this in turn reduced the extent of steam reforming and water gas shift reactions resulting in a decreased H_2 content and increased CH_4 and CO content of the product stream. Finally, the process reached the post breakthrough phase when the completely saturated sorbent no longer played any role in the process, leaving active only the steam reforming and WGS reactions. Here, the outlet composition was close to the equilibrium of conventional steam reforming, although the measured CO_2/CO ratio was moderately lower than expected, possibly due to some residual deviation from equilibrium of WGS reaction.

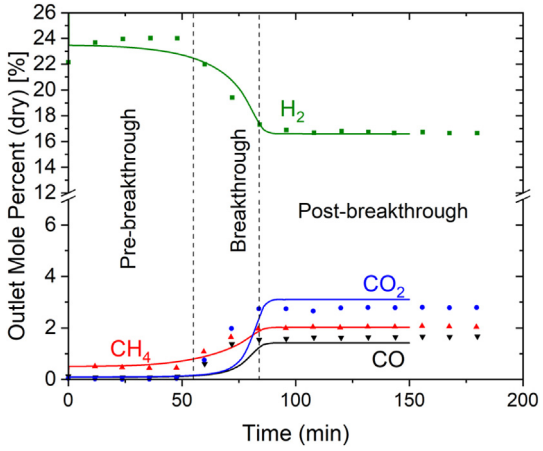

Fig. 1 – Simulation of SER lab-scale test. Solid lines: model; Symbols: experimental data from Balasubramanian et al. [43] Reactor outlet species mole fraction (dry basis), Green: H_2, Red: CH_4, Blue: CO_2, and Black: CO. Vertical dashed lines: Reaction temporal phases.

The model correctly described the observed evolution of phases; from the pre-breakthrough phase to the post-breakthrough, the dynamic transition between phases and the values of the species concentrations are close to the measured data. The calculated concentration of the major species, hydrogen, and methane, keep almost constant during about 50 min; then a slight drop of the hydrogen content coupled with an increase in the methane content develops and evolves into the breakthrough phase, where the simulated hydrogen and methane molar fractions compare well with the experimental values. In this central phase, the simulated trends of the carbon oxides describe with lower accuracy the experimental values; the simulated profiles of both CO_2 and CO are in fact significantly sharper and delayed. However, the duration of breakthrough phase is well captured. The mismatch between the experimental and simulated CO_X breakthrough could be explained by the specific features of the sorbent used in the experimental work. The post-breakthrough region is properly captured by the model; the calculated flat profiles match the thermodynamic equilibrium of steam reforming, thus slightly deviate from the non-equilibrated experimental data.

Considering the complexity of the experiment and the reasonable but several assumptions made about the thermal behavior, the kinetics of chemical reactions and the properties of solids, the comparison between predicted and measured trends appear satisfactory.

Simulation of a full-scale reactor under reference conditions

The model was then used to evaluate the feasibility of the sorption enhanced reforming of methane in a full scale adiabatic fixed bed reactor (2.26 m diameter, 5 m length) to produce highly concentrated streams of hydrogen in a single step. Following the approach proposed in [44], a thermodynamic study was performed and a base case was selected to evaluate the process at a pressure of 10 bar with a steam to carbon ratio of 4 and a feeding temperature of 550 °C. These working conditions were selected to maintain the temperature high enough to thermodynamically favor the methane reforming, and simulate the system far from the possible formation of $Ca(OH)_2$ that hinders the H_2 yield and the carbon capturing performance as reported in [44]. The initial solid temperature was assumed at 700 °C, higher than the feed temperature, to simulate a previous high temperature regeneration step. For simplicity, the reactor was also assumed to be initially filled with steam and H_2 mixture. As a basis of calculation, a feed flow rate of 1 ton/h of methane (350 $Nm^3_{CH4}/h/m^2$) was assumed, which corresponds to a GHSV = 350 $Nm^3/h/m^3_{reactor}$ or 2.12 $Nm^3/h/kg_{cat}$. The simulations were performed assuming that the reactor was packed with sorbent and catalyst particles of 1 mm diameter at a volumetric sorbent to catalyst ratio of 5. At these conditions, a very low Biot number was calculated which validated the isothermal particles' assumption. The reactor geometrical characteristics, selected to minimize the pressure drop by limiting the maximum superficial velocity at 0.2 m/s and to reduce the vessel cost by keeping a proper length to diameter ratio, and operating parameters used for the simulation of the benchmark case are presented in Table 1.

Table 1 – Reactor characteristics and operating conditions for the reference case.

Feed gas temperature	550	°C
Initial solids temperature	700	°C
Pressure	10	Bar
Steam to carbon molar ratio	4	mol/mol
Inlet molar composition	20% CH_4; 80% H_2O	%mol
Inlet gas flow rate	7000	Nm^3/h
Sorbent to catalyst ratio	5	m^3_{CaO}/m^3_{Cat}
Catalyst particle density	1650	kg/m^3
Sorbent particle density	1650	kg/m^3
Reactor diameter	2.26	m
Reactor length	5	m
Particle diameter ($d_{particle}$)	1	mm
GHSV	350	$Nm^3/h/m^3_{reactor}$
Max sorbent conversion (X_{max})	0.4	mol_{caco3}/mol_{cao}
Catalyst effectiveness factor (η)	0.3	–
Void fraction* (ε)	0.4	–

*Calculated according to equation S1 of Section B of the Supplementary Material.

Fig. 2 reports the calculated dynamics of temperature and composition at the reactor outlet after injection of the feed at time zero. In a very short time (12s) the initial gas volume filling the reactor is completely displaced and product distribution at reactor outlet (dry basis) suddenly changes from the initial condition (100% H_2) to the pre-breakthrough one.

After the almost instantaneous gas displacement, the adiabatic conditions and the assumption of pre-heated bed here simulated result in a four-phase dynamic evolution. Firstly, a highly steady stream is predicted to exit the reactor with constant temperature and composition, defining the pre-breakthrough period. The duration of this phase is mainly controlled by the heat capacity of the reactor bed, keeping the outlet temperature constant, and the sorption capacity of the reactor, pushing high the extent of the reforming and WGS reactions. After about 2800s the reactor enters in a thermal breakthrough phase characterized by an initial temperature decline; however, a steep temperature increase occurs at about 5000s, after which the outlet temperature keeps above 650 °C for about 2500s. As better illustrated below, this temperature rise is associated with the exothermic CO_2 sorption in the moving carbonation zone of the bed. At the approaching full saturation of the sorbent, the CO_2 breakthrough occurs, accompanied by CH_4 breakthrough and the decline of H_2 concentration and temperature. Finally, the reactor enters the post breakthrough phase when the sorbent is completely saturated and no longer plays any role in the process; the reactor acts then as a conventional methane reformer under adiabatic condition.

A better understanding of the reactor outlet response can be obtained by examining the evolution of the axial profiles of temperature and composition in Figs. 3 and 4. Notably, multiple phenomena occur simultaneously and produce a complex behavior: the heat transfer between the preheated solid and the incoming gas, the fast and highly endothermic steam reforming process, the progressive and highly exothermic sorbent carbonation.

As soon as the feeding mixture is introduced, the colder inlet gas temperature and the endothermic reforming

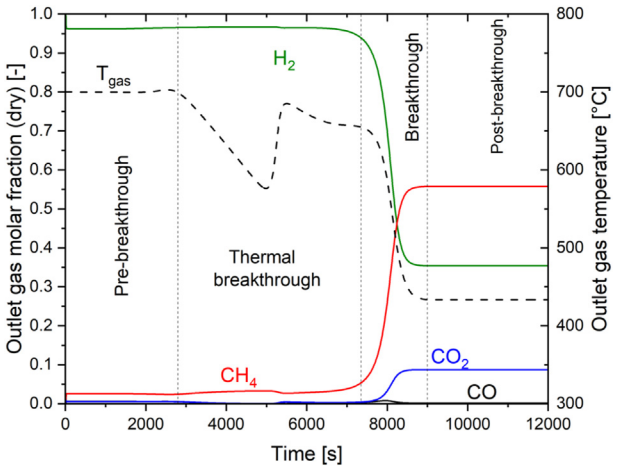

Fig. 2 – Typical breakthrough curves of methane SER. Working conditions: P = 10 bar; S/C = 4; T_{feed} = 550 °C; $T_{bed,\ initial}$ = 700 °C. Left axis: solid lines: Reactor outlet species mole fractions (dry basis), Green: H_2, Red: CH_4, Blue: CO_2, and Black: CO. Right axis: Dashed line: Reactor outlet gas stream temperature.

reactions (that take place on the catalyst) cool down the bed inlet. Here, carbonation of the sorbent starts, and its growing extent (Fig. 4A) affects the gas phase composition, until reaching of the local full saturation state within about 1000s. This produces a shift of the sorption process downstream, such that two reaction fronts form: a fully equilibrated steam reforming front at the reactor inlet and a SER front that moves along the bed, driven by the carbonation of the solid. This explains the steep changes of concentration of gas-phase species that also migrate across the bed.

Since methane is partly converted to COx at the reactor inlet, in the SER front the rate of carbonation exceeds the rate of steam reforming, as shown in Fig. 5; here the axial evolution of calculated rates is plotted at two characteristic time steps, in the pre-breakthrough and in the thermal breakthrough phases. The unbalance between exothermic CO_2 capture and endothermic methane consumption produces a local temperature increase that, like a wave, travels towards the reactor outlet. This phenomenon overlaps with the progressive cooling of the solid, which moves through the bed with a speed governed by the ratio of the solid to flowing gas heat capacity [37], determining the complex evolution of outlet temperature at the reactor exit observed in the thermal break-through phase.

Eventually, the carbonation front in the solid phase reaches the reactor outlet producing the CO_2-breakthrough. The reactor turns then into an equilibrated steam reformer with a unique inlet reaction front.

Fig. 3B, which reports the temperature difference between the solid phases and the gas along the reactor at different time steps, shows positive peaks in the sorbent phase associated with the exothermic carbonation reaction and negative peaks in the catalyst phase associated with endothermic steam reforming, evidencing that the gas phase effectively acts as the heat transfer medium between the catalyst and the sorbent phases, equalizing the temperature of the two solid phases.

Process key performance indices

The overall performances of the large-scale reactor were evaluated based on a set of key performance indices defined by integrating over time the inlet and outlet molar flow rates from the start of CH_4 feeding to the breakthrough time (BTt); this was selected as the time required to reach an outlet CO_2 molar fraction of 0.01 on dry basis. The selected KPI were: the integral methane conversion (Eq. (24)), the hydrogen yield defined as the ratio of the produced H_2 moles over the theoretical maximum from complete methane conversion and WGS (Eq. (25)), the hydrogen purity (Eq. (26)), the Carbon Capture Ratio (CCR) defined as the ratio between number of carbon atoms trapped in the reactor and the number of carbon atoms fed over the duration of the process (Eq. (27)), the sorbent bed

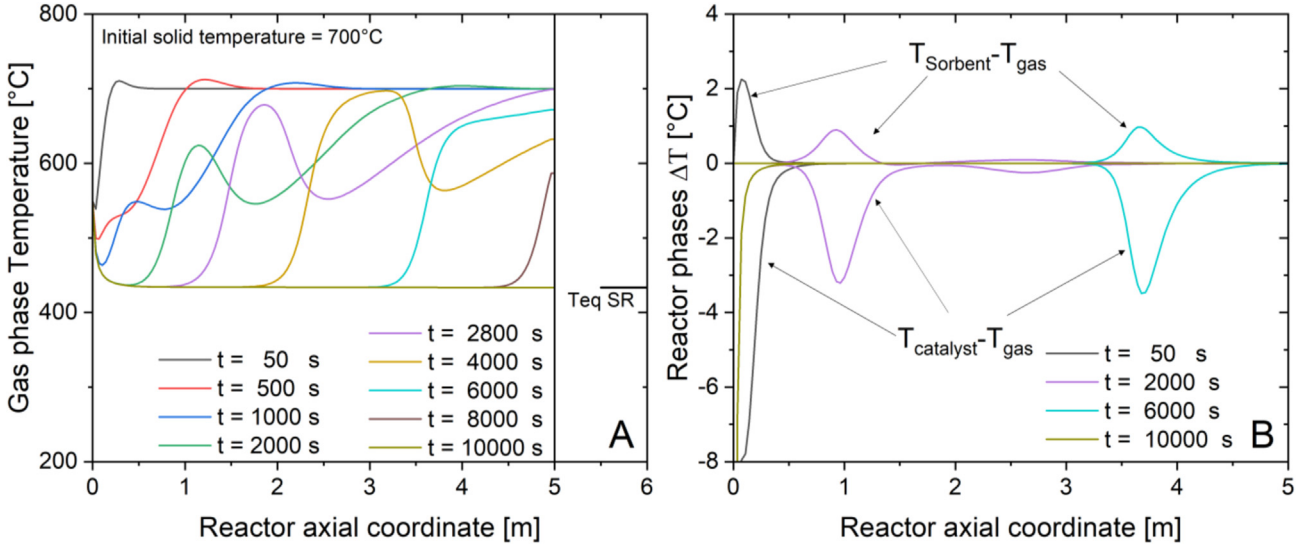

Fig. 3 – Typical dynamic axial profiles of temperature for methane SER process in adiabatic fixed bed reactor. Working conditions: P = 10 bar; S/C = 4; T_{feed} = 550 °C; $T_{bed,\ initial}$ = 700 °C.

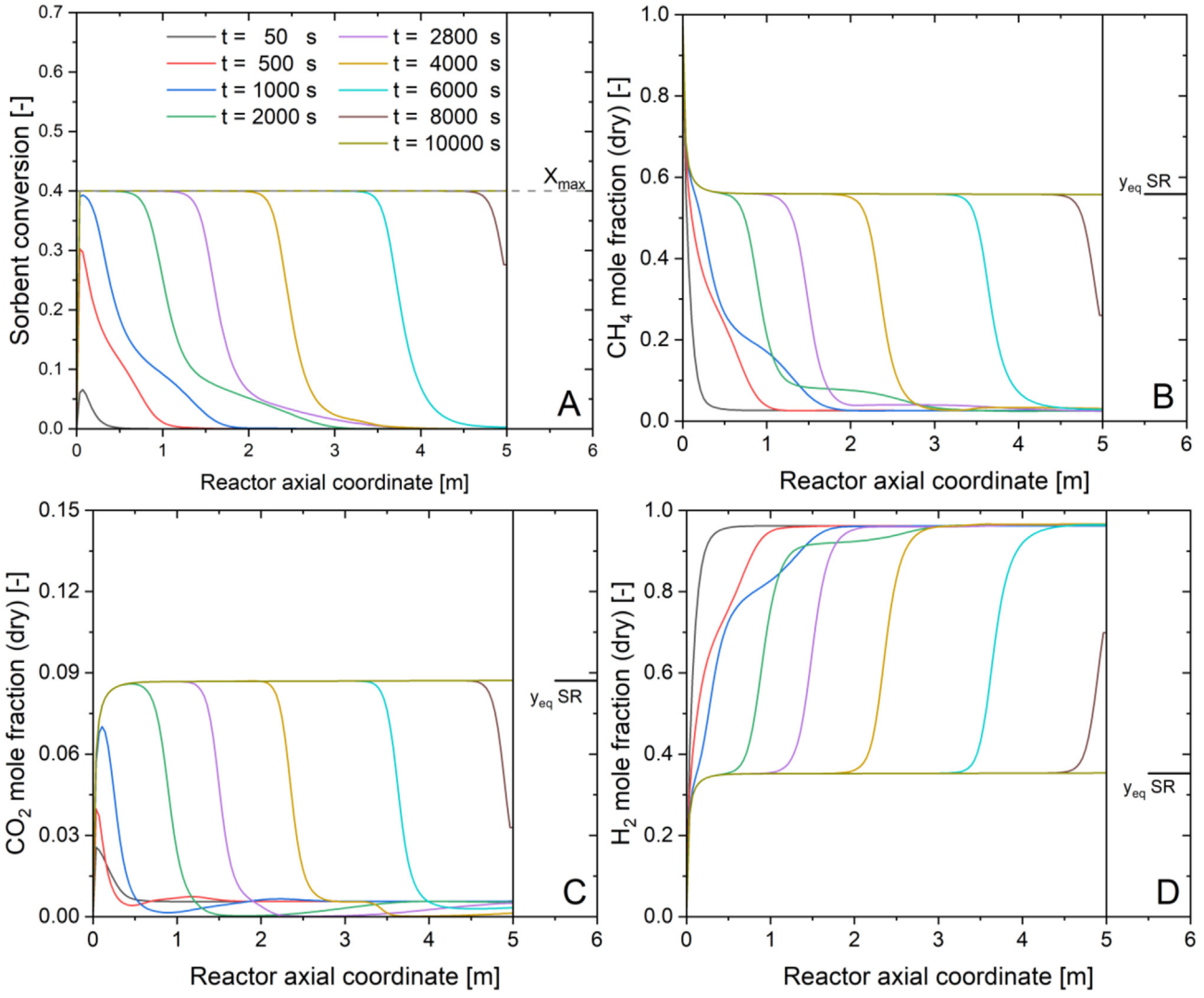

Fig. 4 – Typical dynamic axial profiles of composition for methane SER process in adiabatic fixed bed reactor. Working conditions: P = 10 bar; S/C = 4; T_{feed} = 550 °C; $T_{bed,\ initial}$ = 700 °C.

utilization defined as the ratio between the number of converted and initial CaO moles at breakthrough time (Eq. (28)).

$$Integral\ CH_4\ conversion = \frac{\int_0^{BTt} \dot{n}\ CH_4^{in}\,dt - \int_0^{BTt} \dot{n}\ CH_4^{out}\,dt}{\int_0^{BTt} \dot{n}\ CH_4^{in}\,dt} \quad (24)$$

$$Integral\ hydrogen\ yield = \frac{\int_0^{BTt} \dot{n}\ H_2^{out}\,dt}{4^* \int_0^{BTt} \dot{n}\ CH_4^{in}\,dt} \quad (25)$$

$$Integral\ Hydrogen\ purity = \frac{\int_0^{BTt} \dot{n}\ H_2^{out}\,dt}{\int_0^{BTt} \dot{n}\ total^{out}\,dt - \int_0^{BTt} \dot{n}\ H_2O^{out}\,dt} \quad (26)$$

$$Integral\ carbon\ capture\ ratio\ (CCR) = \frac{\int_0^{BTt} NC_i \dot{n}_i^{gas\ in}\,dt - \int_0^{BTt} NC_i \dot{n}_i^{gas\ out}\,dt}{\int_0^{BTt} NC_i \dot{n}_i^{gas\ in}\,dt} \quad (27)$$

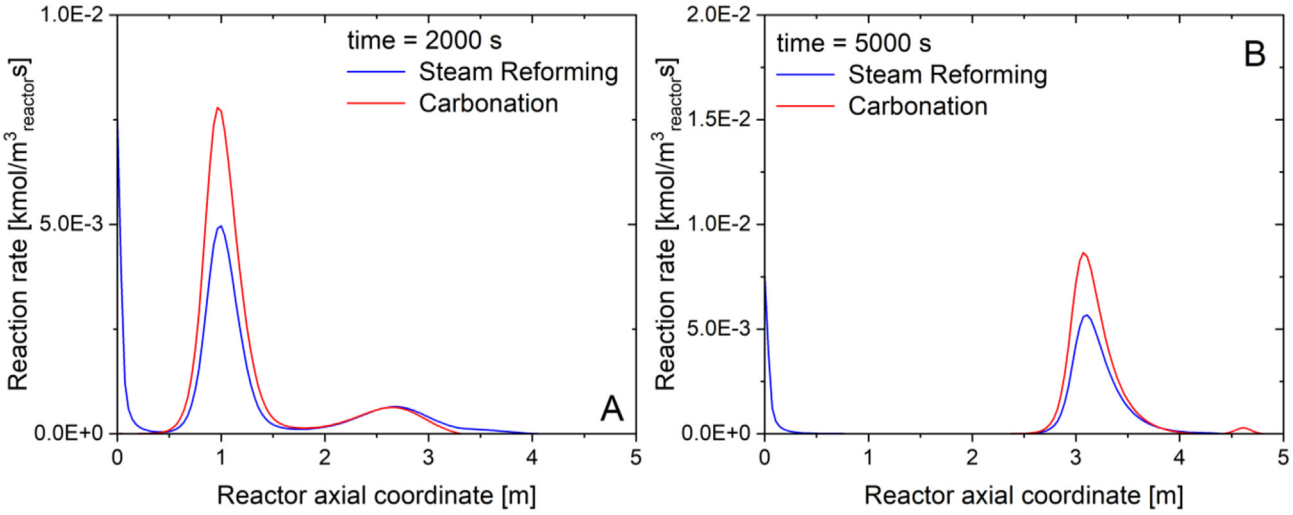

Fig. 5 – Dynamic axial profiles of rates of reaction. Working conditions: P = 10 bar; S/C = 4; T_{feed} = 550 °C; $T_{bed,\ initial}$ = 700 °C.

$$Sorbent\ bed\ utilization = \frac{\int_0^L n_{CaCO_3}(BTt)dz}{\int_0^L n_{CaO}(t=0)dz} \quad (28)$$

As reported in Table 2, at the reference conditions discussed above, the SER reformer grants an overall CH_4 conversion of 88.6%, capturing 85.9% of the feed carbon and yielding 87.5% of the maximum theoretical H_2 production in a stream with an overall purity of 96.1%. Looking at the uncaptured carbon containing species (representing 14.1% of the total feed carbon), only 19.3% of them slipped out in the form carbon oxides while the remaining 80.7% is unconverted methane. It is worth mentioning that 38.4% of the CaO is converted at the selected breakthrough criteria; this corresponds to 97% of the active CaO considering that the maximum conversion was set to be 40%. Simulations performed at higher space velocity show that such high performances can be maintained up to GHSV = 875 $Nm^3/h/m^3_{reactor}$ corresponding to a 2.5-fold intensification of the SER process. Detailed simulation results at varying GHSV are reported in Section G of the Supplementary Material.

Table 2 also reports the evaluation of the performance's indices across the duration of the single pre-breakthrough and thermal breakthrough phases; notably, better performances are predicted during the pre-breakthrough phase. This analysis clearly shows the negative effect of the temperature drop during the thermal breakthrough region, that limits the CH_4 conversion and hinders the overall performance of the process. At the same time, the results show that the pre-breakthrough phase has a major role in the process, sustaining a steady flow of pure H_2 and providing high CO_2 capturing performance.

This suggests that a strategy for improving the SER performance passes through the optimization of the reactor thermal behavior. A parametric analysis was thus addressed (and is presented in the following paragraphs) on the effects of key operating and design parameters such as the inlet gas temperature, the initial solid temperature, the heat capacity of the fixed bed.

In this respect, it is important to observe that since the SER process dynamically switches between two independent steps (reforming and regeneration) and regeneration is highly favored at elevated temperatures, the thermal capacity of the fixed bed (that is the heat stored in the hot solids at the end of the regeneration) open degrees of freedom for optimizing the following reforming stage.

Parametric analysis

The thermal behavior of the reactor is herein studied by varying the parameters related to the heat carriers, gas (the inlet gas temperature) and solid bed (initial temperature and heat capacity), playing a role in the SER process.

Effect of the inlet gas temperature

Keeping all the other parameters constant, the feed gas temperature was varied between 450 °C and 600 °C. It is evident from the breakthrough curves plotted in Fig. 6, that the variation of the feed temperature has no effect on the pre-breakthrough phase, where the process is mainly driven by the heat capacity of the bed. The main impact of the feed temperature is visible along the thermal breakthrough phase, where the assumed increasing feed temperature limits the reduction of the outlet gas temperature and sustains higher methane conversion, which results in lower methane and higher hydrogen concentration in the outlet gas. In turn, the higher conversion of methane obtained on increasing the feed temperature leads to faster saturation of the sorbent shortening the material breakthrough time. As the post-breakthrough acts as an adiabatic conventional methane steam reformer, the feed temperature sets the thermodynamic limitation for the methane conversion and hydrogen yield during this phase. Consistently with the

Table 2 – Overall performance indices of the benchmark case.

	Pre-Breakthrough (t = 0 → 2800)	Thermal Breakthrough (t = 2800 → 7720)	Overall (t = 0 → 7720)
CH_4 conversion	90.6%	87.5%	88.6%
Hydrogen yield	88.9%	86.7%	87.5%
Hydrogen purity	96.3%	96.0%	96.1%
Carbon capture ratio	86.4%	85.7%	85.9%
Sorbent bed Utilization	13.9%	24.5%	38.4%
Uncaptured carbon distribution			
CH_4	68.9%	87.1%	80.7%
CO	15.9%	6.0%	9.4%
CO_2	15.2%	6.9%	9.9%

breakthrough profiles, Fig. 6 shows that the overall methane conversion, the hydrogen yield and purity, and the CCR increase with the feed temperature, particularly in the 450 °C–500 °C range.

It is worth noting that the increase of the feed temperature results in higher risk of coke formation before the catalytic bed entrance, which puts a warning to the present analysis. On the other hand, reducing the feed temperature will lead to

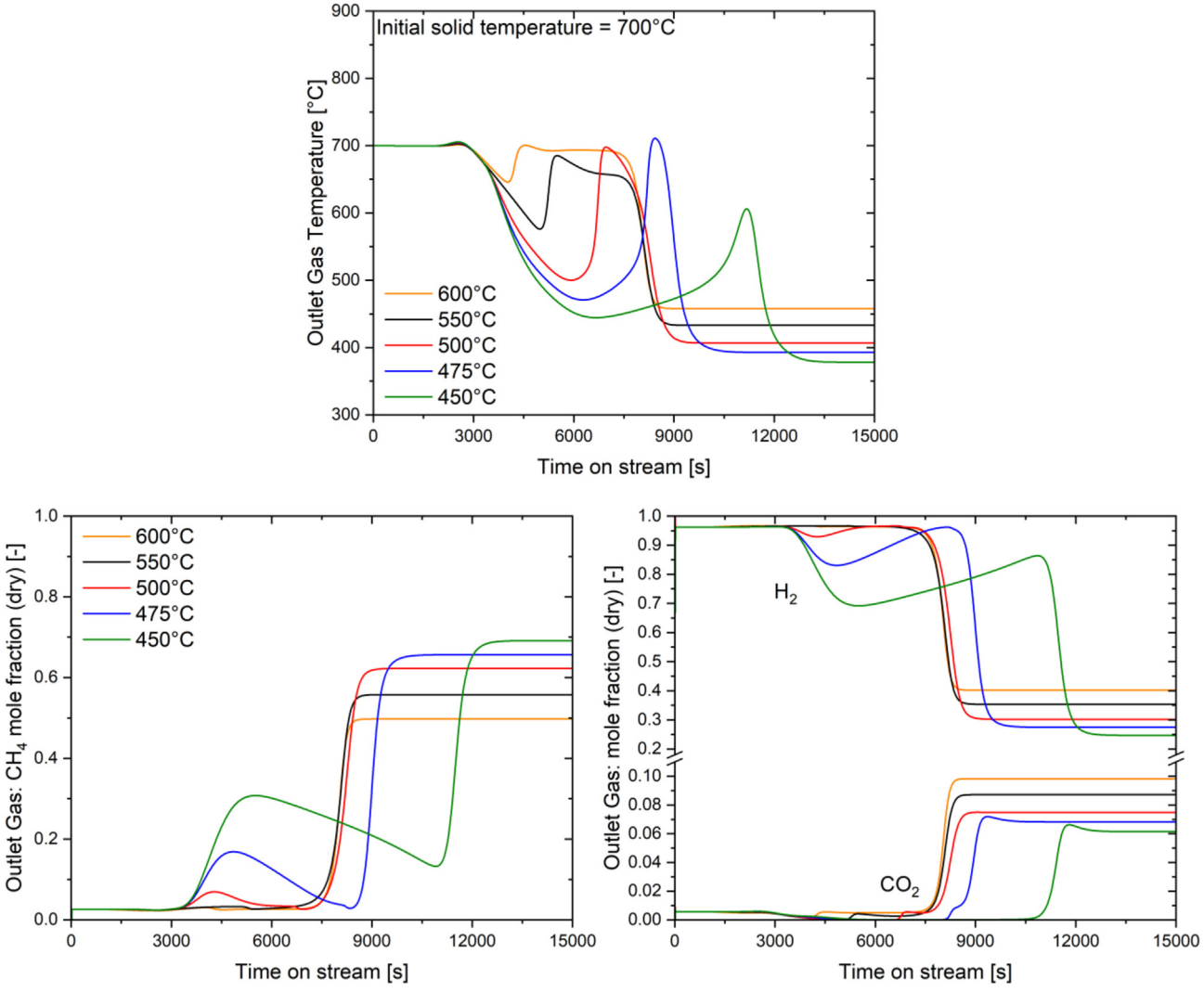

Fig. 6 – Effect of the feed temperature on the breakthrough curves for methane SER. Working conditions: P = 10 bar; S/C = 4; $T_{bed,\ initial}$ = 700 °C. T_{feed} = *Green*: 450°C, Blue: 475 °C, *Red*: 500°C, *Black*: 550°C, Orange: 600 °C.

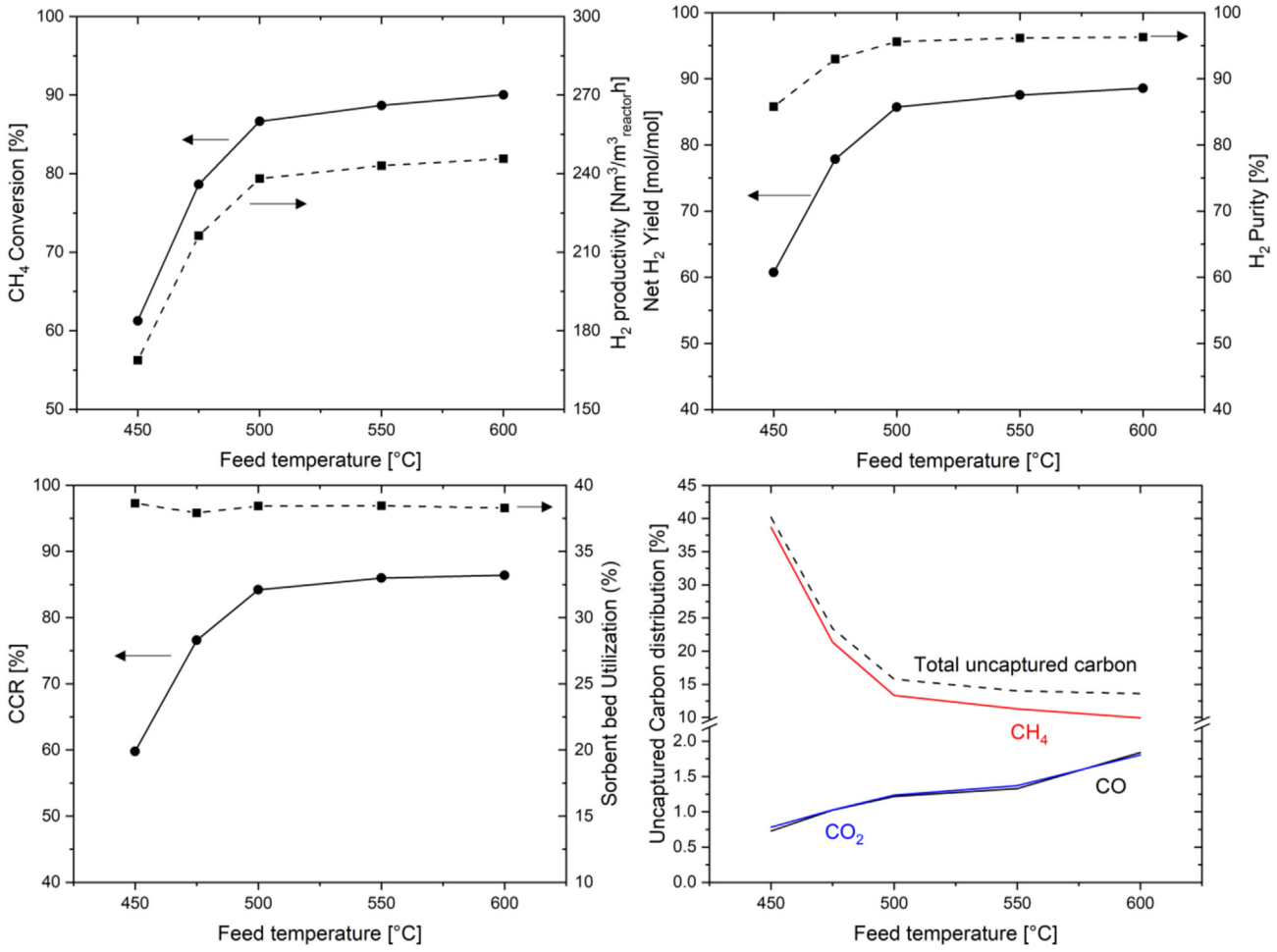

Fig. 7 – Effect of the feed temperature on the integral performances of the methane SER process. Working conditions: P = 10 bar; S/C = 4; $T_{bed,\ initial}$ = 700 °C.

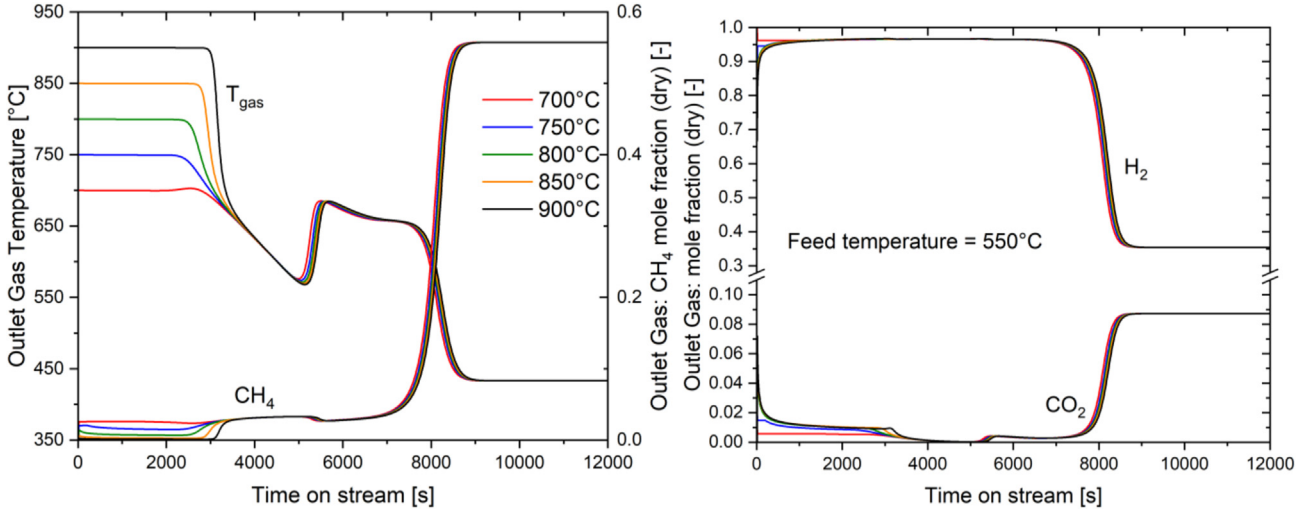

Fig. 8 – Effect of the initial bed temperature on the breakthrough curves for methane SER. Working conditions: P = 10 bar; S/C = 4; T_{feed} = 550 °C. $T_{bed,\ inital}$ = Red: 700 °C, Blue: 750 °C, Green: 800 °C, Orange: 850 °C, Black: 900 °C.

regions where the temperature of unconverted CaO will be low enough to thermodynamically favor the hydration reaction. For the purpose of this analysis the effect of the hydration reaction was not considered.

The effect of the feed temperatures on the overall process was evaluated by calculating the KPI calculated according to Eqs. 24–28. As reported in Fig. 6, the feed temperature has no effect on the pre-breakthrough phase and only affects the thermal breakthrough phase. As reported in Fig. 7, a significant improvement of the SER performance on increasing the feed temperature from 450 °C to 600 °C is shown; indeed, methane conversion was predicted to grow from 61.3% to 86.6% and the CCR from 59.8% to 84.3%. The effect becomes less important on further increasing the feed temperature up to 600 °C, which increases the methane conversion to 90% and the CCR to 86.4%. Hydrogen purity follows the same trend raising from 85.8% at 450 °C to 95.6% at 500 °C and finally up to 96.3% at 600 °C feed temperature.

Table 3 – Effect of the initial bed temperature on the integral performance indices after 2000 s, i.e. within the pre-breakthrough period (Working conditions: P = 10 bar; S/C = 4; T_{feed} = 550 °C).

	$T_{bed,\ inital}$ = 700 °C	$T_{bed,\ inital}$ = 800 °C	$T_{bed,\ inital}$ = 900 °C
CH_4 conversion	90.5%	96.9%	99.5%
Hydrogen yield	88.6%	93.4%	95.0%
Hydrogen purity	96.3%	95.6%	95.2%
Carbon capture ratio	86.2%	83.2%	81.0%
Bed Utilization	9.96%	9.60%	9.35%
Uncaptured carbon distribution			
CH_4	69.0%	18.5%	2.8%
CO	15.9%	51.0%	68.0%
CO_2	15.1%	30.5%	29.2%

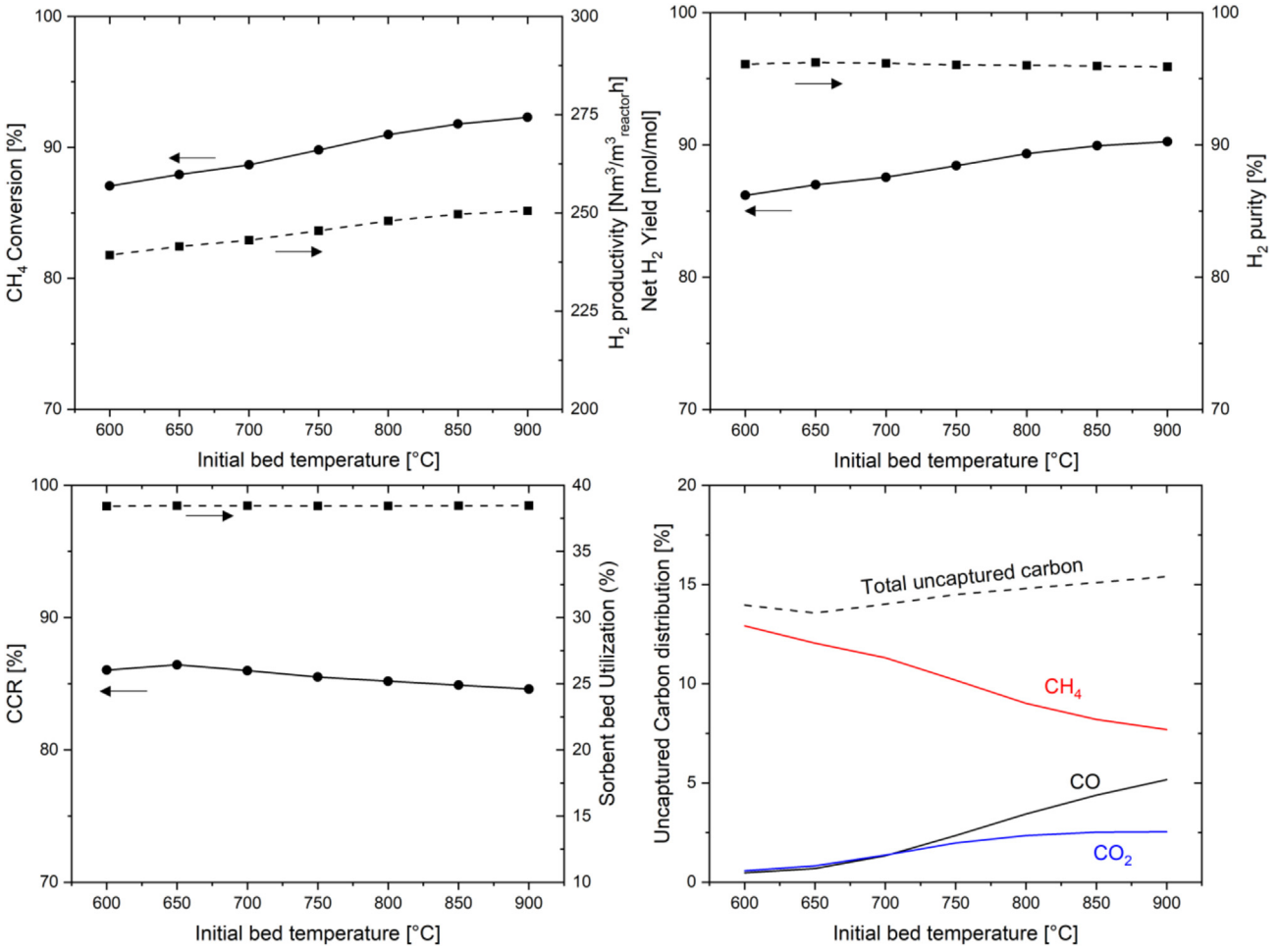

Fig. 9 – Effect of the initial bed temperature on the integral performances of the methane SER process. Working conditions: P = 10 bar; S/C = 4; T_{feed} = 550 °C.

Effect of the bed initial temperature

The effect of varying the initial bed temperature in a range between 600 °C and 900 °C was calculated while keeping the feed temperature at 550 °C. The highest selected temperature of 900 °C is significant as it is representative of the expected bed temperature after the regeneration phase, occurring at atmospheric pressure without any sweep gas. As presented in Fig. 8, the initial bed temperature has a clear effect during the pre-breakthrough phase when the process is controlled by the bed's heat capacity, leading to a higher methane conversion with the increase of the initial bed temperature. However, the high temperature limits thermodynamically the CO_2 sorption reaction, which results in higher content of carbon oxides that leave the reactor. On the other hand, no effect of the initial bed temperature is predicted for the thermal breakthrough, the material breakthrough, and post breakthrough phases.

Looking at the effect of the initial bed temperature on the overall process, the KPIs were calculated after 2000 s i.e. within the pre-breakthrough period. The results of this calculation, as presented in Table 3, clearly show an improved methane conversion rising from 90.5% to 99.5% on increasing the initial bed temperature from 700 °C to 900 °C; on the other hand, the CCR drops from 86.2% to 81.0%. Additionally, the composition of the uncaptured carbon is dominated by unconverted methane at the initial bed temperature of 700 °C and more CO is expected at higher initial bed temperature resulting from lower extent of WGS reaction resulting from the higher bed temperature and the lower extent of the carbonation reaction consuming the CO_2.

Extending the calculation over the complete breakthrough time (pre-breakthrough + thermal breakthrough) as presented in Fig. 9, an attenuated effect of the initial bed temperature on the SER performance is predicted. The hydrogen yield increases from 86% up to 90% following the increase of the methane conversion and the CCR slightly declines from 86% to 84%. This result indicates that the SER process can be

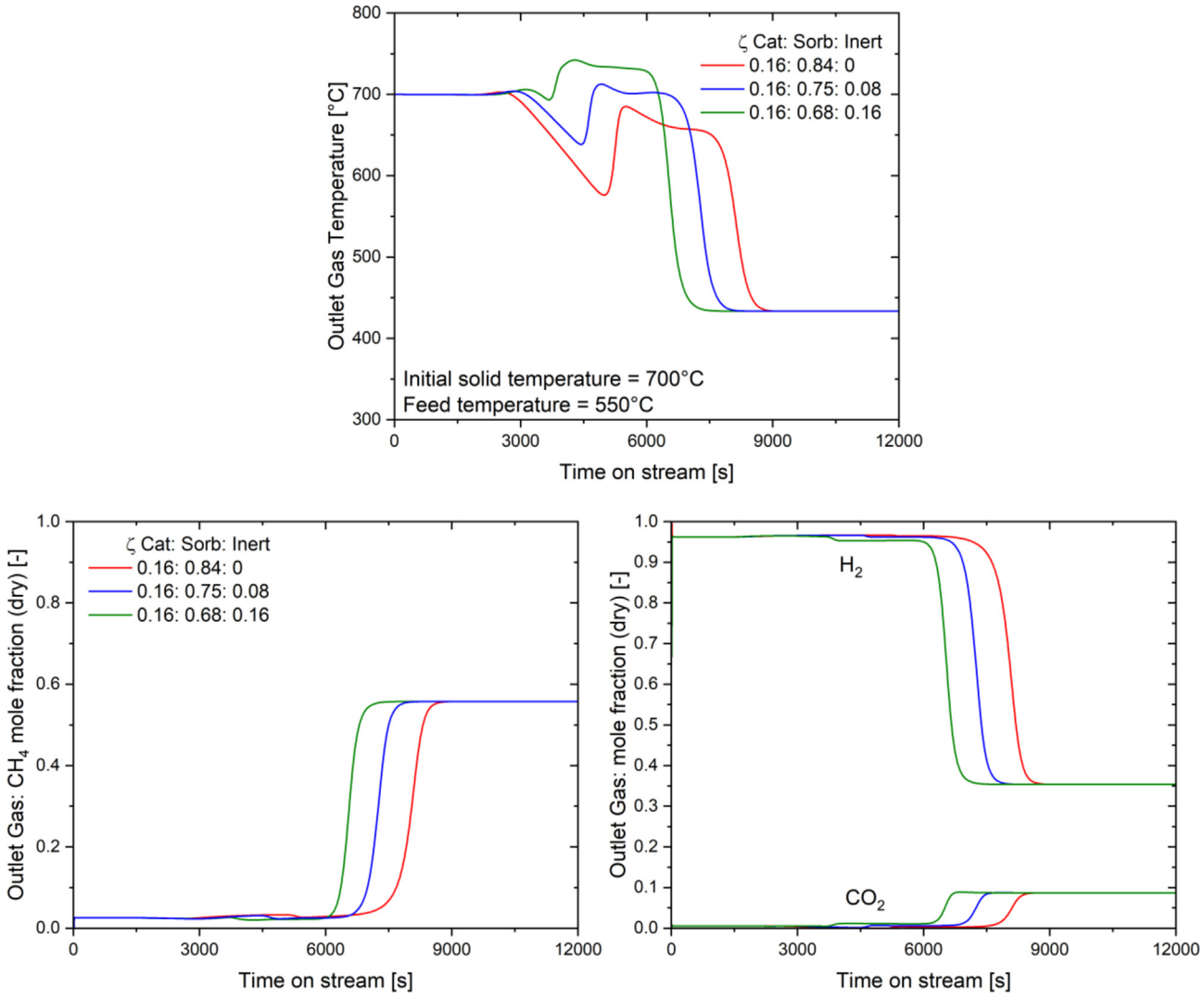

Fig. 10 – Effect of inert heat carrier addition on the breakthrough curves for methane SER. Working conditions: P = 10 bar; S/C = 4; $T_{bed,\ initial}$ = 700 °C. T_{feed} = 550 °C. ξ_{inert} = Red: 0, Blue: 0.08, Green: 0.16.

operated at high performance when minimizing or eliminating the cooling down step after the sorbent regeneration step: on the one side, there is a beneficial effect of the bed thermal capacity on the reforming step, on the other side the operation of the whole process cycle is greatly simplified.

Effect of inert heat carrier addition

The aforementioned results clearly show that the time lag between the thermal and material breakthroughs severely affects the overall SER performance. In order to better balancing the heat and CO_2 capture capacities of the fixed bed, replacement of a fraction of sorbent with inert pellets was simulated. Commercial alumina pellets of the of the same particle size of the catalyst and the sorbent were selected as they present suitable low cost solution for increasing the heat capacity of the reactor (high density $\rho_{inert} = 3950\ kg/m^3$, and similar specific heat capacity to the catalyst and the sorbent $Cp_{inert} = 0.88\ kJ/kgK$). By replacing part of the sorbent with the alumina pellets, a double effect is expected: an increase of the bed's thermal capacity with a consequent delay of the thermal breakthrough and a reduction of the sorbent stock in the reactor and consequently of the material breakthrough time.

While keeping the catalyst volume fraction of the reference case with no inert addition, 10% and 20% of the sorbent volume was replaced with the inert material, corresponding to an inert bed volumetric fraction of 8% and 16% respectively. Simulations were performed at reference operating conditions (P = 10 bar; S/C = 4; T_{feed} = 550 °C; $T_{bed,\ initial}$ = 700 °C; GHSV = 350 $Nm^3/m_{rec}{}^3h$).

The calculated breakthrough curves presented in Fig. 10 show that the moderate increase of the bed thermal capacity slightly extends the pre-breakthrough phase, characterized by a relatively constant outlet gas temperature. Moving to the thermal breakthrough phase, the simulated outlet stream temperature significantly increases with the inert solid fraction, leading to higher methane conversion. Remarkably at the highest simulated inert fraction the outlet temperature during the thermal breakthrough phase significantly exceeds the initial solid temperature. Similar results were reported in the literature [22]. Using a pseudo homogeneous model Martini et al. investigated a modified SER process where the reactor was loaded with catalyst, sorbent and Cu pellets, this latter acting as an inert during the reforming step; investigating the impact of different operating conditions, temperature profiles

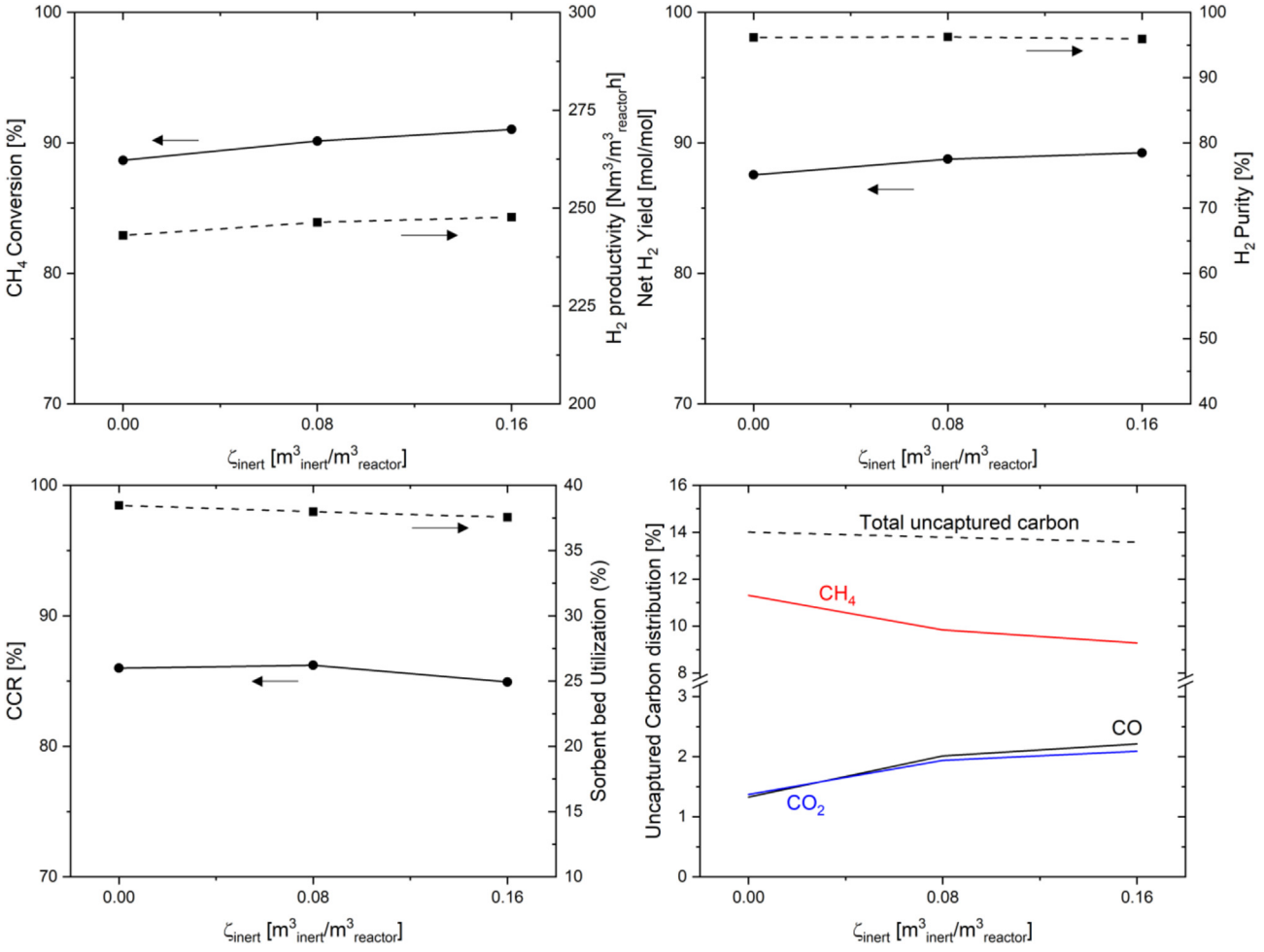

Fig. 11 – Effect of inert heat carrier addition on the integral performances of the methane SER process. Working conditions: P = 10 bar; S/C = 4; T_{feed} = 550 °C; $T_{bed,\ initial}$ = 700 °C.

with a maximum temperature exceeding the initial bed temperature were obtained even though the SER process is globally endothermic.

Finally, the increasing amount of inert in the bed brings forward the breakthrough, as a result of the reduction of the sorption capacity of the reactor and the increase of conversion in the thermal breakthrough phase.

The effect of progressive replacement of sorbent with inert material on the integral process KPI is presented in Fig. 11. Results of this analysis show that the overall methane conversion improves with the inert solid fraction (from 88.6% to 91.0%), leading to higher hydrogen yield and higher carbon capture ratio. However, this strategy leads to a marked reduction of the breakthrough time, thus increased number of reaction-regeneration cycles leading to some possible technical hurdles. A basic energy analysis for the three cases was performed by calculating the specific heat required to regenerate the reactor bed at 900 °C. Results of this analysis show that the specific heat required for the sorbent regeneration stage grows from 0.279 MJ/MJ_{H2} to 0.307 MJ/MJ_{H2} on replacing 20% of the sorbent with the inert. Details about this analysis are reported in section H of the Supplementary Material. Therefore, a global technoeconomic analysis of the process, including the full cycle reaction-regeneration and heat recovery, is required to better assess the benefit of addition of inert solids in the bed on the overall plant KPIs. It is worth mentioning that additional simulations were performed at a lower feed temperature of 450 °C to magnify the role of the thermal bed capacity in the process and the results can be found in section I of the Supplementary Materials of this work. The axial profiles for the highly diluted case are presented in section I of the Supplementary Material as well.

Similar effects to those calculated for addition of inert material were found when studying the impact of the maximum sorbent conversion (X_{max}), where the inactive portion of the sorbent acts as an inert to the process. This indicates that the degradation of the sorbent during the cyclic behavior of the process has positive effect on the performance of the process in terms of CH_4 conversion and carbon capture ratio but reduces the cycle time and worsens the energy efficiency. Results of X_{max} effect are reported in Section J of Supplementary Material of this work together with those of a sensitivity analysis on the second carbonation kinetic parameter, k_{carb}.

Conclusions

Methane sorption enhanced reforming (SER) process in a fixed bed reactor under adiabatic conditions was modelled in this work using a 1-D heterogeneous model. The model accounts for three well mixed solid phases: the sorbent, the catalyst, and the inert, in addition to the gas phase, providing crucial information on the role of each of the phases on the thermal behavior of the reactor and the global performance of the SER process. The proposed SER model was based on the kinetic expressions published in the literature that describe the main reactions involved in the process and was validated using experimental results from the literature. Simulations covering a wide range of operating parameters were carried out with the aim of providing comprehensive understanding and interpretation of their effects on the technical KPIs, namely: methane conversion, hydrogen yield and purity, and carbon capture ratio (CCR).

Results of model simulations highlighted the need of a sufficient enthalpy input to compensate for the endothermic nature of the methane SER process at high temperatures. Higher CH_4 conversion and carbon capture ratios were simulated on increasing either the feed temperature, the initial solid temperature, or the bed heat capacity. From an energy efficiency aspect, feed gas preheating is preferable if achieved through waste heat recovery, on the other hand, it may result in high heat exchangers cost and other technical issues (e.g. coke formation).

The initial bed temperature was shown to have a minor effect on the global performance of the SER process over the duration of the reforming step. An increase of the H_2 yield from 86.1% to 90.2% was calculated on increasing the initial bed temperature from 700 °C to 900 °C, counteracted by a slight drop in the CCR by 1.4% (from 86% to 84.6%) on increasing the initial bed temperature from 700 °C to 900 °C. However, this result indicates the potential to avoid or minimize the extent of a cooling step between regeneration and reforming stages with beneficial implications on the overall efficiency of the process.

Increasing the bed heat capacity, thus the energy stored in the bed from the regeneration step by the addition of inert material, avoids the coking issues but leads to an increase in the heat demand for bed regeneration, reducing the overall energy efficiency of the process with a predicted increase of about 10% (from 0.279 MJ/MJ_{H2} to 0.307 MJ/MJ_{H2}) on replacing 20% of the sorbent with dense alumina pellets.

Declaration of competing interest

The authors declare that they have no known competing financial interests or personal relationships that could have appeared to influence the work reported in this paper.

Acknowledgements

Abdelrahman Mostafa gratefully acknowledge ENI S.P.A for the financial support under the PhD scholarship agreement with Politecnico di Milano.

Appendix A. Supplementary data

Supplementary data to this article can be found online at https://doi.org/10.1016/j.ijhydene.2023.03.357.

Nomenclature

$a_{V,j}$	Phase j specific surface area per unit volume [m^2/m^3]
A	Reactor cross sectional area [m^2]

BTt	Breakthrough time [s]
$C_{j,i}$	Phase j molar concentration of species i [kmol/m^3]
Cp_g	Specific heat capacity of the gas [kJ/kg/K]
Cp_i	Specific heat capacity of species i, (i = CaO, $CaCO_3$) [kJ/kg/K]
$Cp_{sorbent}$	Specific heat capacity of the sorbent [kJ/kg/K]
d_p	Particle diameter [m]
$D_{ae,i}$	Effective axial dispersion of species i [m^2/s]
$F_{gas,tot}$	Total specific molar flow rate [mol/m^2/s]
G	Mass flow velocity [kg/m^2/s]
h_{gs}	Gas-solid heat transfer coefficient [kW/m^2/K]
$k_{m,i}$	Gas-solid mass transfer coefficient of species i [m/s]
k_{carb}	rate constant of CaO carbonation [s^{-1}]
L_t	Total reactor length [m]
MW_{gas}	Gas mixture molar weight [kg/kmol]
MW_i	Molar weight of species i [kg/kmol]
n_i	Number of moles of species i [kmol]
$\dot{n}_i$	Molar flow rate of species i [kmol/s]
NC_i	Number of carbon atoms in species i [–]
P	Total pressure [MPa]
$p_{co_2,eq}$	Equilibrium CO_2 partial pressure [atm]
R_j	Rate of reaction j [kmol/kg$_{catalyst}$/s]
R_{carb}	Rate of carbonation [kmol/kg$^0_{CaO}$/s]
$S_{P,j}$	Geometric particle surface area of solid j [m^2]
T_j	Temperature of phase j [K]
U	Superficial velocity of gas [m/s]
$V_{P,j}$	Particle volume of solid j [m^3]
$X_{sorbent}$	Fractional sorbent conversion [mol$_{CaCO_3}$/mol$_{CaO}$]
X_{max}	Maximum sorbent conversion [mol$_{CaCO_3}$/mol$_{CaO}$]
$y_{gas,i}$	Gas phase molar fraction of species i [–]
$y_{co_2,eq}$	Equilibrium molar fraction of CO_2 [-]
Z	Axial coordinate of the bed [m]

Greek letters

ε	Bed void fraction [–]
$\Delta H_{R,j}$	Heat of reaction j [J/mol]
ΔH_{carb}	Heat of carbonation reaction [J/mol]
μ_g	Viscosity of the gas [MPa s]
$\rho_{Catalyst}$	Catalyst particle density [kg/m^3]
ρ_{CaO}	Initial sorbent particle density [kg/m^3]
ρ_{inert}	Inert particle density [kg/m^3]
ρ_g	Gas density [kg/m^3]
$\rho_{sorbent}$	Sorbent bed density at time t [kg/m^3]
ξ_j	Volumetric fraction of solid phase j [m^3_j/m$^3_{solid}$]
η	Catalyst effectiveness factor [–]
ν_{ij}	Stoichiometric coefficient of species i in reaction j [–]
λ_{ax}	Effective axial thermal conductivity [kW/m/K]

REFERENCES

[1] Harrison DP. Sorption-enhanced hydrogen production: a review. Ind Eng Chem Res Sep. 2008;47(17):6486–501. https://doi.org/10.1021/ie800298z.

[2] Gil MV, Fermoso J, Rubiera F, Chen D. H2 production by sorption enhanced steam reforming of biomass-derived bio-oil in a fluidized bed reactor: an assessment of the effect of operation variables using response surface methodology. Catal Today 2015;242:19–34. https://doi.org/10.1016/j.cattod.2014.04.018.

[3] International energy outlook 2021. 2021 [Online]. Available: https://www.eia.gov/pressroom/presentations/AEO2021_Release_Presentation.pdf.

[4] Gul H, Arshad MY, Tahir MW. Production of H2 via sorption enhanced auto-thermal reforming for small scale Applications-A process modeling and machine learning study. Int J Hydrogen Energy 2023;xxxx. https://doi.org/10.1016/j.ijhydene.2022.12.217.

[5] Di Nardo A, Calchetti G, Di Carlo A, Stendardo S. Sorption enhanced steam methane reforming in a bubbling fluidized bed reactor: simulation and analysis by the CPFD method. Comput Chem Eng 2023;169(November 2022):108080. https://doi.org/10.1016/j.compchemeng.2022.108080.

[6] Sheu WJ, Chu CS, Chen YC. The operation types and operation window for high-purity hydrogen production for the sorption enhanced steam methane reforming in a fixed-bed reactor. Int J Hydrogen Energy 2022;47(88):37192–203. https://doi.org/10.1016/j.ijhydene.2021.11.112.

[7] Yan Y, et al. Process simulations of blue hydrogen production by upgraded sorption enhanced steam methane reforming (SE-SMR) processes. Energy Convers Manag 2020;222(June):113144. https://doi.org/10.1016/j.enconman.2020.113144.

[8] Scaltsoyiannes AA, Lemonidou AA. On the factors affecting the deactivation of limestone under calcium looping conditions: a new comprehensive model. Chem Eng Sci 2021;243:116797. https://doi.org/10.1016/j.ces.2021.116797.

[9] Di Giuliano A, Gallucci K. Sorption enhanced steam methane reforming based on nickel and calcium looping: a review. Chem. Eng. Process. - Process Intensif. 2018;130(May):240–52. https://doi.org/10.1016/j.cep.2018.06.021.

[10] Iliuta MC. CO 2 sorbents for sorption-enhanced steam reforming. In: Advances in chemical engineering. 51. Academic Press Inc.; 2017. p. 97–205.

[11] Wang Y, et al. A review of CO2 sorbents for promoting hydrogen production in the sorption-enhanced steam reforming process. Int J Hydrogen Energy 2021;46(45):23358–79. https://doi.org/10.1016/j.ijhydene.2021.01.206.

[12] Sikarwar VS, et al. Progress in in-situ CO2-sorption for enhanced hydrogen production. Prog Energy Combust Sci June 2021;91:2022. https://doi.org/10.1016/j.pecs.2022.101008.

[13] Teixeira P, Bacariza C, Correia P, Pinheiro CIC, Cabrita I. Hydrogen production with in situ CO2 capture at high and medium temperatures using solid sorbents. Energies 2022;15(11):1–44. https://doi.org/10.3390/en15114039.

[14] Barin I. Thermochemical data of pure substances 1997;55(4).

[15] hua Xiu G, Li P, Rodrigues AE. Sorption-enhanced reaction process with reactive regeneration. Chem Eng Sci 2002;57(18):3893–908. https://doi.org/10.1016/S0009-2509(02)00245-2.

[16] Lee DK, Baek IH, Yoon WL. Modeling and simulation for the methane steam reforming enhanced by in situ CO2 removal utilizing the CaO carbonation for H2 production. Chem Eng Sci 2004;59(4):931–42. https://doi.org/10.1016/j.ces.2003.12.011.

[17] Li ZS, Cai NS. Modeling of multiple cycles for sorption-enhanced steam methane reforming and sorbent regeneration in fixed bed reactor. Energy Fuel 2007;21(5):2909–18. https://doi.org/10.1021/ef070112c.

[18] Sheu WJ, Chang CY, Chen YC. Transient reaction phenomena of sorption-enhanced steam methane reforming in a fixed-bed reactor. Int J Hydrogen Energy 2022;47(7):4357–74. https://doi.org/10.1016/j.ijhydene.2021.11.088.

[19] Fernandez JR, Abanades JC, Murillo R. Modeling of sorption enhanced steam methane reforming in an adiabatic fixed bed reactor. Chem Eng Sci 2012;84:1–11. https://doi.org/10.1016/j.ces.2012.07.039.
[20] Abbas SZ, Dupont V, Mahmud T. Modelling of H2 production in a packed bed reactor via sorption enhanced steam methane reforming process. Int J Hydrogen Energy 2017;42(30):18910–21. https://doi.org/10.1016/j.ijhydene.2017.05.222.
[21] Abbas SZ, Dupont V, Mahmud T. Modelling of H 2 production via sorption enhanced steam methane reforming at reduced pressures for small scale applications. Int J Hydrogen Energy 2019;44(3):1505–13. https://doi.org/10.1016/j.ijhydene.2018.11.169.
[22] Martini M, Martínez I, Romano MC, Chiesa P, Gallucci F, van Sint Annaland M. Increasing the carbon capture efficiency of the Ca/Cu looping process for power production with advanced process schemes. Chem Eng J 2017;328:304–19. https://doi.org/10.1016/j.cej.2017.07.048.
[23] Martini M, van den Berg A, Gallucci F, van Sint Annaland M. Investigation of the process operability windows for Ca-Cu looping for hydrogen production with CO2 capture. Chem Eng J 2016;303:73–88. https://doi.org/10.1016/j.cej.2016.05.135.
[24] Ergun S. Fluid flow through packed columns. Chem Eng Prog 1952;48:89–94.
[25] Ochoa-Fernández E, Rusten HK, Jakobsen HA, Rønning M, Holmen A, Chen D. Sorption enhanced hydrogen production by steam methane reforming using Li2ZrO3 as sorbent: sorption kinetics and reactor simulation. Catal Today 2005;106(1–4):41–6. https://doi.org/10.1016/j.cattod.2005.07.146.
[26] Bhatia SK, Perlmutter DD. The effect of pore structure on fluid-solid reactions: application to the SO2-lime reaction. AIChE J Mar. 1981;27(2):226–34. https://doi.org/10.1002/aic.690270209.
[27] Pfeffer R. Heat and mass transport in multiparticle systems. Ind Eng Chem Fundam 1964;3(4):380–3. https://doi.org/10.1021/i160012a018.
[28] Wakao N, Kaguei S, Nagai H. Effective diffusion coefficients for fluid species reacting with first order kinetics in packed bed reactors and discussion on evaluation of catalyst effectiveness factors. Chem Eng Sci 1978;33(2):183–7. https://doi.org/10.1016/0009-2509(78)85052-0.
[29] J.P.O. Bruce E. Poling, John M. Prausnitz, The properties of gases and liquids, 5th ed. McGraw-Hill Professional, 2000.
[30] Fuller EN, Ensley K, Giddings JC. Diffusion of halogenated hydrocarbons in helium. The effect of structure on collision cross sections. J Phys Chem 1969;73(11):3679–85. https://doi.org/10.1021/j100845a020.
[31] Specchia V, Baldi G, Sicardi S. Heat transfer in packed bed reactors with one phase flow. Chem Eng Commun 1980;4(1–3):361–80. https://doi.org/10.1080/00986448008935916.
[32] Mcbride B, Gordon S, Reno M. Coefficients for calculating thermodynamic and transport properties of individual species. NASA Tech Memo 1993;4513. NASA-TM-4513, p. 98, http://ntrs.nasa.gov/archive/nasa/casi.ntrs.nasa.gov/19940013151_1994013151.pdf.
[33] Xu J, Froment GF. Methane steam reforming, methanation and water-gas shift: I. Intrinsic kinetics. AIChE J 1989;35(1):88–96. https://doi.org/10.1002/aic.690350109.
[34] Abanades JC, Alvarez D. Conversion limits in the reaction of CO2 with lime. Energy Fuel 2003;17(2):308–15. https://doi.org/10.1021/ef020152a.
[35] Fang F, Li ZS, Cai NS. Experiment and modeling of CO2 capture from flue gses at high temperature in a fluidized bed reactor with ca-based sorbents. Energy Fuel 2009;23(1):207–16. https://doi.org/10.1021/ef800474n.
[36] Cai J, Wang S, Kuang C. Modeling of carbonation reaction for CaO-based limestone with CO2 in multitudinous calcination-carbonation cycles. Int J Hydrogen Energy 2017;42(31):19744–s. https://doi.org/10.1016/j.ijhydene.2017.06.173.
[37] Bhatia SK, Perlmutter DD. Effect of the product layer on the kinetics of the CO2-lime reaction. AIChE J Jan. 1983;29(1):79–86. https://doi.org/10.1002/aic.690290111.
[38] Grasa G, Murillo R, Alonso M, Abanades JC. Application of the random pore model to the carbonation cyclic reaction. AIChE J May 2009;55(5):1246–55. https://doi.org/10.1002/aic.11746.
[39] Mess D, Sarofim AF, Longwell JP. Product layer diffusion during the reaction of calcium oxide with carbon dioxide. Energy Fuel 1999;13(5):999–1005. https://doi.org/10.1021/ef980266f.
[40] Rodríguez N, Alonso M, Abanades JC. Experimental investigation of a circulating fluidized-bed reactor to capture CO2 with CaO. AIChE J May 2011;57(5):1356–66. https://doi.org/10.1002/aic.12337.
[41] Erans M, Manovic V, Anthony EJ. Calcium looping sorbents for CO2 capture. Appl Energy 2016;180:722–42. https://doi.org/10.1016/j.apenergy.2016.07.074.
[42] Baker EH. The calcium oxide–carbon dioxide system in the pressure range 1—300 atmospheres. 87 J Chem Soc 1962:464–70. https://doi.org/10.1039/JR9620000464.
[43] Balasubramanian B, Ortiz AL, Kaytakoglu S, Harrison DP. Hydrogen from methane in a single-step process. Chem Eng Sci 1999;54:3543–52.
[44] Romano MC, Cassotti EN, Chiesa P, Meyer J, Mastin J. Application of the Sorption Enhanced-Steam Reforming process in combined cycle-based power plants. Energy Proc 2011;4:1125–32. https://doi.org/10.1016/j.egypro.2011.01.164.